Journal of Materials Chemistry C

ROYAL SOCIETY OF CHEMISTRY

PAPER

View Article Online
View Journal | View Issue

Cite this: J. Mater. Chem. C, 2023, 11, 8045

Bio-inspired micro area concentrated array assisted perovskite photodetector toward weak light imaging†

Lutong Guo,[ab] Kun Zhang,[ab] Mingquan Tao,[ab] Rudai Zhao,[a] Tingqing Wu,[ab] Yang Wang *[ab] and Yanlin Song *[ab]

Received 7th September 2022,
Accepted 31st October 2022

DOI: 10.1039/d2tc03760b

rsc.li/materials-c

Perovskite photodetectors (PVK PDs) have emerged as weak-light imaging devices due to their favorable carrier mobility, induced light absorption, and photoelectric performance. Modifying the optical structure is an effective strategy for improving the light-collecting performance and sensitivity of the device. Here, a designed and fabricated bio-inspired micro-area concentrated perovskite photodetector system with a micro hemisphere structured array exhibits superior capabilities in light harvesting, and achieves excellent PD device electrical performance and weak light imaging. The responsivity (R) and detectivity (D^*) of the micro area concentrated PVK PD reach 0.2 A W^{-1} and 1.37 $\times$ 10^{13} Jones, which are 16.4 and 11.7 times higher than that of the pristine material. The on/off ratio of the micro area concentrated PVK PD is up to 1.6 $\times$ 10^4. The micro hemisphere structured array of PD significantly enhances the weak light sensitivity and results in the realization of weak light imaging under 0.64 μW cm^{-2}.

10th Anniversary Statement

Journal of Materials Chemistry C is an excellent journal. We have published several articles in *Journal of Materials Chemistry C*, which represent the frontiers of our scientific research and exploration. Meanwhile, we also obtain exciting new ideas and experimental processes from *Journal of Materials Chemistry C*. In the perovskite photodetector, modifying the optical structure is a simple and convenient way to improve the electrical performance and weak light imaging. In this manuscript, we have designed and fabricated a bio-inspired micro-area concentrated perovskite photodetector system with an array with a micro hemisphere structure, which significantly enhances the weak light sensitivity and realizes weak light imaging under 0.64 μW cm^{-2}.

Introduction

Extensive attention has been paid to organic–inorganic hybrid perovskites (PVKs) as photodetectors due to their favorable carrier mobility, induced light absorption, and photoelectric performance,[1–6] which are suitable for application to weak light imaging,[7–9] night vision systems[10] and underwater operations.[11] However, current improvement methods mainly include increasing the exposure time and reducing the operating temperature, which do not change the sensitivity of the detector itself under weak light. Some literature studies report methods such as adding electron transport layers and passivating defects to improve perovskite photodetector performance,[12] ignoring the harvesting of weak light. Therefore, designing and constructing optical structures is key to improving the photoresponse performances of the device.[13] Fortunately, inspiration can be taken from animals with night vision:[14] owls have more rod cells in the retina and a large curvature of the cornea, and a lens allowing more light to converge into the eye, achieving night vision even in a weak light environment. A bio-inspired optical structure as an effective strategy can enhance the light-collecting performance and sensitivity (weak light) of the perovskite photodetector.

Herein, we propose a bio-inspired perovskite ($MAPbI_3$) photodetector for weak light detection with an array of micro hemisphere structures (called 600 nm-PVK PD), utilizing the bio-inspired micro hemisphere structures to achieve a high light concentration in a small space for weak light detection and imaging. The bio-inspired micro area concentrated array can achieve high light harvesting and absorb more reflected light from the back glass. Moreover, a confined crystallization

[a] Key Laboratory of Green Printing, Institute of Chemistry, Chinese Academy of Sciences, Beijing National Laboratory for Molecular Sciences, CAS Research/Education Center for Excellence in Molecular Sciences, Zhongguancun North First Street 2, 100190, Beijing, P. R. China
[b] School of Chemical Science, University of Chinese Academy of Sciences, 100190, Beijing, P. R. China. E-mail: wangyang@iccas.ac.cn, ylsong@iccas.ac.cn

† Electronic supplementary information (ESI) available. See DOI: https://doi.org/10.1039/d2tc03760b

method *via* nanoimprinting facilitates the PVK crystallinity and reduces the defects, improving the electrical properties of the photodetector devices.[15] Therefore, the micro area concentrated 600 nm-PVK PD obtains a responsivity (0.20 A W^{-1}) and detectivity (1.37 $\times$ 10^{13} Jones) 16.4 and 11.7 times those of the pristine material, and the on/off ratio is up to 1.6 $\times$ 10^{4}. The 600 nm-PVK PD can achieve weak light imaging under low light intensity (0.64 μW cm^{-2}).

Results and discussion

Fig. 1 shows the bio-inspired micro area concentrated perovskite photodetector, which has been fabricated by nanoimprinting (Fig. 1a). The 2D photo crystals (PCs) with different-sized templates (180 nm, 600 nm and 900 nm) are fabricated using an air–water interface self-assembly method[16] (Fig. S1, ESI†).

A schematic of the fabrication process of imprinted photodetectors is depicted in the experimental section and ESI† (Fig. S2). After peeling off the PDMS, the pattern of the 2D PC becomes a tessellation of hexagons, because this is the closest-packed structure of a spherical array[17] (Fig. S3, ESI†). The perovskite films with micro area concentrated structures are named the 180 nm-perovskite (180 nm-PVK), 600 nm-perovskite (600 nm-PVK), 900 nm-perovskite (900 nm-PVK), and flat-perovskite (Flat-PVK) (Fig. S4 and S5, ESI†). This bio-inspired micro area concentrated structure ensures the light harvesting ability and optoelectrical properties.[18]

In Fig. 1b, the light intensity has been modified by the attenuator, realizing a strong response under low light intensity and weak light imaging (Fig. 1c and d). Moreover, under the same large curvature structure, the effect of light enrichment depends on the wavelength. Due to refraction and Bragg's law of reflection, the optical structure has the best light-concentration efficiency at the half-wavelength of the light. The optical structures such as the lens structure have different interactions with different wavelengths, and the focus positions of the structures with different sizes are also different. The parallel light at different intervals satisfies the Bragg diffraction formula during reflection. Therefore, for $MAPbI_3$, 650 nm incident light is the ideal excitation wavelength for the photodetector. In the nano-imprinting process, a complete hemisphere structure cannot actually be formed, so the hemisphere size compared with the 600 nm template is about 2/3 of the original (400 nm), which meets the requirement for the half-wavelength of the incident light when compared with 900 nm and 180 nm. The 600 nm-perovskite film exhibits higher absorbance compared with the pristine material (Fig. 2a). In Fig. 2b and Fig. S6 (ESI†), the main XRD diffraction peaks indicate the pure tetragonal phase.[19] The 600 nm-PVK film with stronger and sharper peaks shows high-quality crystallization, which corresponds to the SEM images in Fig. 2d and Fig. S7 (ESI†). Therefore, the nanoimprinting process can assist the promotion of perovskite crystallization for large crystals and a high-quality perovskite film, which is attributed to the imprinting and gradient annealing facilitating perovskite migration and recrystallization.[20–23] In Fig. S8 (ESI†), the steady-state PL

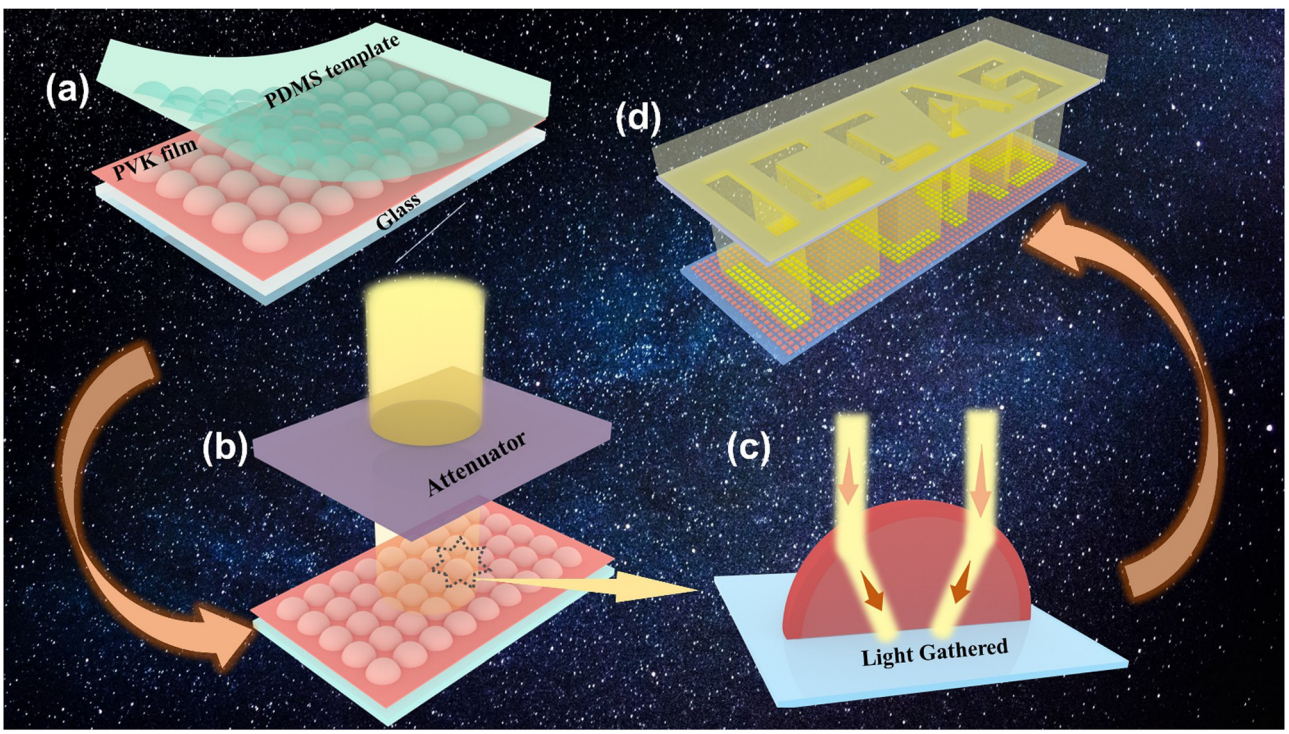

Fig. 1 Schematic of the micro area concentrated perovskite photodetector. (a) Preparation of the micro area concentrated perovskite system. (b) Schematic of light decay. (c) Schematic of light gathering. (d) Weak light imaging by the 600 nm-photodetector.

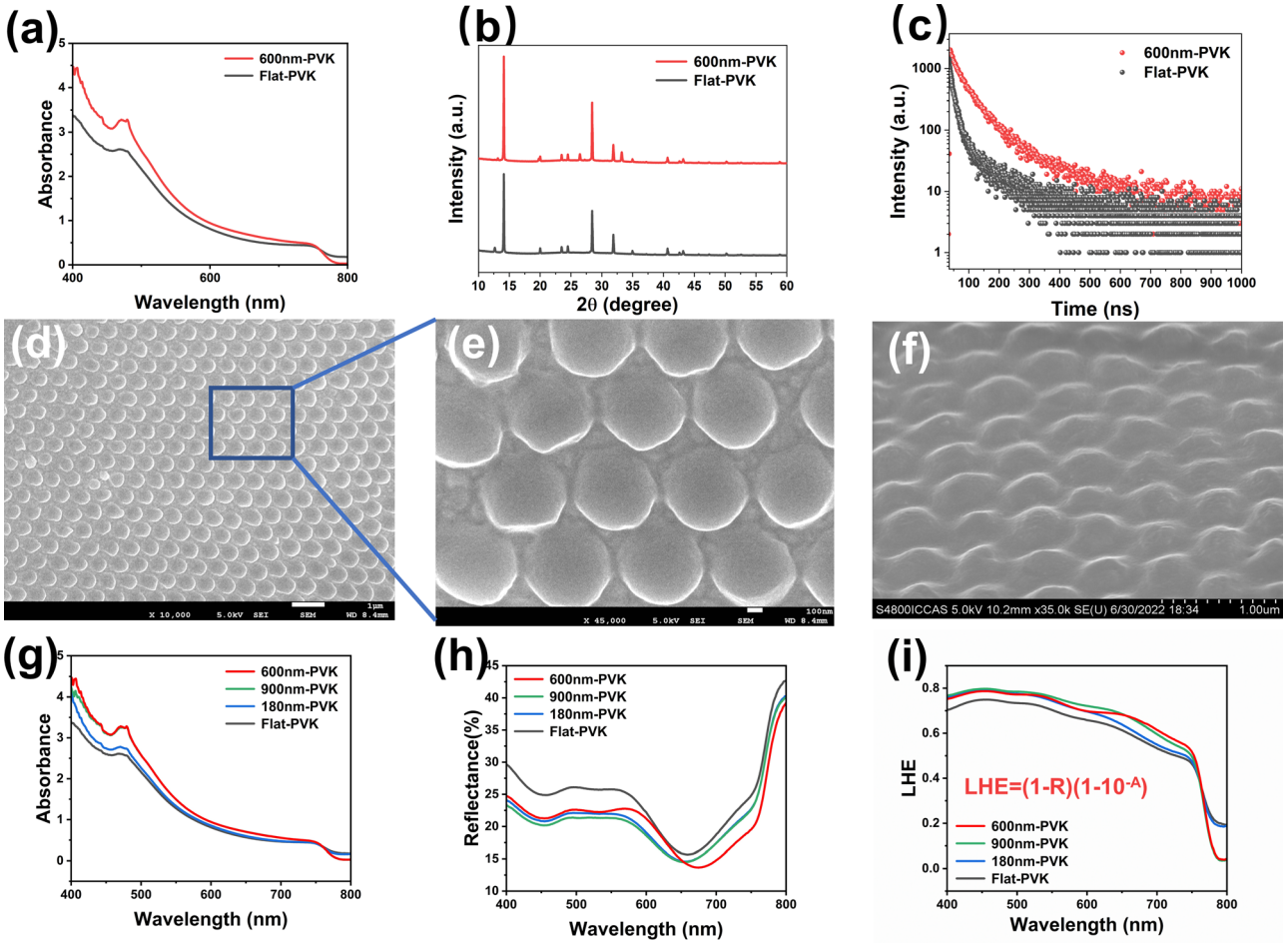

Fig. 2 Characterization of crystallinity and light trapping capability. (a) Absorbance spectra of 600 nm-PVK and Flat-PVK. (b) XRD patterns of 600 nm-PVK and Flat-PVK. (c) Time-resolved photoluminescence of 600 nm-PVK and Flat-PVK. (d) SEM image of the 600 nm-PVK film. (e) Magnified SEM image of the film surface. (f) 45° cross-sectional SEM image of 600 nm-PVK. (g–i) Absorbance spectra, reflectance spectra, and light harvesting efficiency.

spectra of the perovskite films show the same 780 nm emission peak, which shows that the imprinting method has no influence on the perovskite bandgap. In Fig. 2c and Fig. S9 (ESI†), the 600 nm-PVK film shows a longer carrier lifetime (305 ns) than those of the 900 nm-PVK (293 ns), 180 nm-PVK (246 ns), and Flat-PVK (182 ns). The value of the radiative recombination proportion[24] for 600 nm-PVK reaches 84.6% (900 nm-PVK: 82.3%, 180 nm-PVK: 72.8%, Flat-PVK: 76.9%). This further indicates that the 600 nm-PVK film has few surface defects and good crystallization, which are essential for the performance of photodetector devices.[25] Space charge limited current testing (SCLC) measurements are used to quantify the defect states, as shown in Fig. S10 (ESI†). The determined trap-filled limit voltage (V_{TFL}) value of the nano-imprinted device decreases from 0.506 V to 0.292 V, thus the trap density of the nano-imprinted device (7.06×10^{15} cm^{-3}) is lower than that of the pristine material (1.22×10^{16} cm^{-3}). SEM images show that the arrangement of the micro hemisphere structure is orderly (Fig. 2d and e).

The material has good surface morphology and ordered structure even at high magnification, which is proved by the 45° cross-section SEM images (Fig. 2f). Therefore, the constructed bio-inspired micro area concentrated structure can improve the light collection capacity of a unit area. The 600 nm-PVK film obtains a higher absorbance (Fig. 2g) and lower optical reflectance in the 400–800 nm range compared to the pristine material (Fig. 2h). Significantly, the 600 nm-PVK has a higher (11%) light harvesting efficiency (LHE, Fig. 2i) than the pristine material at 650 nm, which favors the weak light imaging of devices under low light intensity. This further demonstrates the effect of the optical structure on light harvesting.[26–28]

Subsequently, the optoelectronic performances of the different perovskite photodetectors (Flat-PD, 180 nm-PD, 600 nm-PD and 900 nm-PD) were measured. A diagram and cross-sectional SEM image are shown in Fig. S11 (ESI†). In Fig. 3a, current–voltage (*I–V*) curves of the Flat-PD and the PDs with 180 nm, 600 nm and 900 nm sized structures in the dark and under illumination (7.98 mW cm^{-2}, 650 nm, 5 V bias) are shown. Due to the bio-inspired micro area concentrated array structure for optical absorption enhancement,[29] there is a 352 nA photocurrent for the 600 nm-PD, which is over 10 times

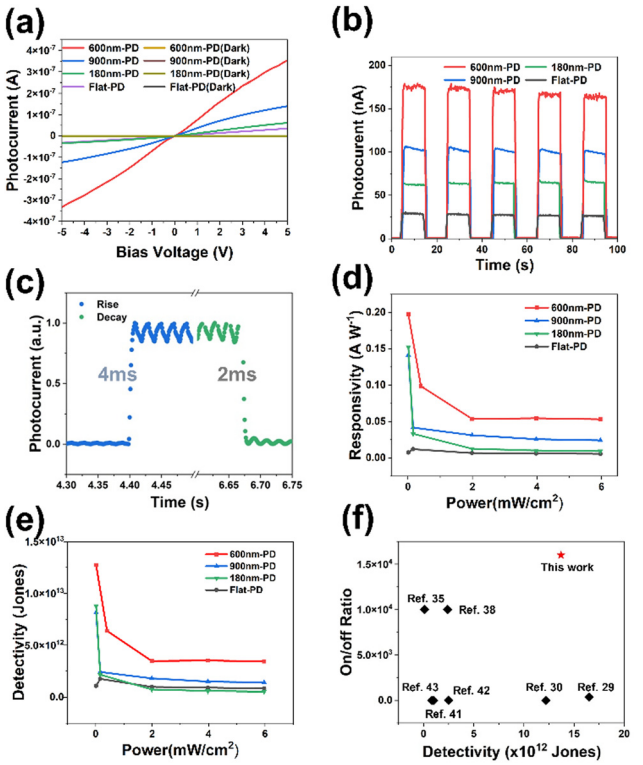

Fig. 3 Photoelectric properties of the perovskite photodetector. (a) *I–V* and (b) *I–t* curves of 600 nm-PD, 180 nm-PD, 900 nm-PD and Flat-PD in the dark and under 5 mW cm^{-2}, 650 nm light illumination at 5 V bias. (c) The response speed curve of 600 nm-PD. (d and e) Responsivity and detectivity curves of 600 nm-PD, 180 nm-PD, 900 nm-PD and Flat-PD under 650 nm light illumination at 5 V bias. (f) Comparison of the detectivity and on/off ratio for $MAPbI_3$ based photodetectors.

that of the Flat-PD (35 nA). *I–V* curves of the 600 nm-PD, 900 nm-PD, 180 nm-PD, and Flat-PD under different amounts of 650 nm light illumination (0.40–7.98 mW cm^{-2}) under 5 V bias voltage (Fig. S12, ESI†) show the same improvement of photocurrent with increasing light intensity. The linear dynamic range shows the linear range of the response to the light intensity for the application of photodetection in a broad light intensity range,[30] and is defined:[31]

$$\mathrm{LDR} = 20\log\frac{I^*_{\mathrm{ph}}}{I_{\mathrm{d}}} \quad (1)$$

where I^*_{ph} is the measured photocurrent under 1 mW cm^{-2}, and I_{d} is the measured current in the dark. Fig. S13 (ESI†) shows the linear relationship between the photocurrent and light intensity of the different PVK PDs. The 600 nm-PD has the higher LDR (57 dB), which is better than the pristine (39 dB) and the other PDs (180 and 900 nm-PDs: 44 dB and 52 dB). Therefore, the micro area concentrated PVK PD (600 nm) exhibits stable photoelectric performance in a broad light intensity range.

In Fig. 3c, the current–time (*I–t*) curves of 600 nm-PD, 900 nm-PD, 180 nm-PD, and Flat-PD show stable light on/off cycles between dark and the light illumination conditions (650 nm, 7.98 mW cm^{-2}) at 5 V bias voltage. The light on/off ratio ($I_{\mathrm{ph}}/I_{\mathrm{d}}$, where I_{ph} is the photocurrent and I_{d} is the dark current)[32–34] is a key parameter and has an influence on the PD photoelectric and imaging performances.[35] The light on/off ratios of 600 nm-PD, 900 nm-PD, 180 nm-PD, and Flat-PD are 6.28×10^3 (I_{ph}: 352 nA, I_{d}: 56 pA), 2×10^3 (I_{ph}: 140 nA, I_{d}: 70 pA), 6.85×10^2 (I_{ph}: 61 nA, I_{d}: 89 pA), and 2.19×10^3 (I_{ph}: 35 nA, I_{d}: 16 pA), as shown in Fig. 3b and Fig. S14 (ESI†). The 600 nm-PD has the largest on/off ratio of 1.6×10^4 (I_{ph}: 113 nA, I_{d}: 7 pA) under white light (Fig. S15, ESI†), and the corresponding response time (rise time: 4 ms, decay time: 2 ms) is shown in Fig. 3c. The responsivity (R), detectivity (D^*) and external quantum efficiency (EQE) are used to evaluate the PD performance. R represents the generated photocurrent per unit area of light intensity,[36–38] which is defined as:

$$R = \frac{I_{\mathrm{ph}} - I_{\mathrm{d}}}{P} \quad (2)$$

where P is the light intensity, and S is the effective area. D^* represents the PD sensitivity affected by thermal fluctuation noise, Johnson noise, and shot noise.[39,40] When the shot noise caused by the dark current dominates D^*, D^* can be simply defined as:

$$D^* = \frac{R\sqrt{S}}{\sqrt{2eI_{\mathrm{d}}}} \quad (3)$$

The external quantum efficiency has been defined[12] as:

$$\mathrm{EQE} = R\frac{hc}{\lambda e} \quad (4)$$

where h, c, λ and e represent the Planck constant, the velocity of light in a vacuum, the wavelength of the light, and the elementary charge, respectively.

Fig. 3d, e and Fig. S16 (ESI†) show the influence of different light intensities from 0.016 to 7.98 mW cm^{-2} on the R, D^*, and EQE of different PDs. The decreasing R value with increasing light intensity indicates that more carriers will recombine under a high light intensity.[41] The trends of D^* and EQE are consistent with the influence of R.[42,43] The values of R, D^* and EQE for the micro area concentrated PVK PD (600 nm) are 0.2 A W^{-1}, 37.77% and 1.37×10^{13} Jones, respectively, which are 16.7, 16.4, and 12.7 times those of the Flat-PD (R: 0.012 A W^{-1}; EQE: 2.31%; D^*: 1.08×10^{12} Jones). Due to the advantages of the constructed bio-inspired micro area concentrated array, the device has a high detection rate and switching ratio compared with other systems in the reported literature (Fig. 3f). The device parameters are summarized in detail and compared with the previously reported $MAPbI_3$ photodetectors in Table S2 (ESI†). The PVK PD exhibits the advantages of a bio-inspired micro area concentrated array to improve the responsivity, directivity, and on/off ratio beyond those reported in the literature.

The bio-inspired micro area concentrated structured photodetector achieves clear weak light imaging under different intensities and wavelengths of light. As shown in Fig. 4a, a mask was placed between the 600 nm-PD and green, red, and blue light sources, and patterned letters "L", "H" and "E", respectively, were transmitted to realize photo-communication.

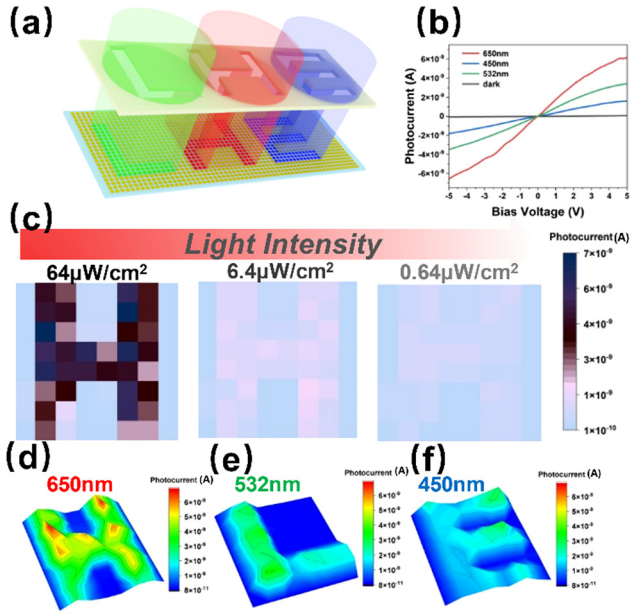

Fig. 4 Characterization of weak light imaging. (a) Schematic of weak light imaging. (b) *I*–*V* curves of 600 nm-PD, in the dark and under 5 mW cm^{-2}, 450 nm, 532 nm and 650 nm light illumination at 5 V bias. (c) Weak light imaging results of letter "H" patterns with different light intensities under 650 nm light illumination at 5 V bias. (d–f) Weak light imaging results of letter "L" "H" and "E" patterns under 64 μW cm^{-2}, 532 nm, 650 nm and 450 nm, respectively, at 5 V bias.

When the size of the optical structure matches the half wavelength of the light, the enrichment effect of the light is better, so the bio-inspired micro area concentrated structured photodetector has different light enrichment capabilities under different wavelengths of light. The 600 nm-PD has the maximum photocurrent under 650 nm light illumination, which is much better than the photocurrents under 532 nm and 450 nm (Fig. 4b). Fig. 4c shows clear weak light imaging even under the weak light intensity of 0.64 μW cm^{-2}. The imaging results indicate visually that the signal-to-noise ratio gradually reduces with decreasing light intensity. Meanwhile, the device also enables muti-wavelength light detection and imaging (Fig. 4d–f). The 600 nm-PD has the best detection (Fig. S17, ESI†) and imaging performance under 650 nm light illumination, which corresponds to the difference in the photocurrent (Fig. 4b). This strategy provides a simple and efficient approach to fabricate high-performance photodetectors for weak light imaging.

Experimental

Stamp fabrication

A PS microsphere colloidal solution (5 wt%) was produced by dispersing in deionized water and ethanol at a 1 : 2 volume ratio. The substrates were put into a clean Petri dish with deionized water. Then, the PS colloidal solution was slowly dripped onto the air–water interface, forming a compact monolayer film assisted by SDS solution. The 2D PC film was transferred to a Si substrate and annealed for 15 min at 80 °C. Finally, PDMS liquid mixed with the pre-polymer and cross-linker was poured onto the 2D PC film and heated at 80 °C for 90 min. The PDMS stamp was obtained after peeling off the 2D PC substrate.

Fabrication of the photodetector

The perovskite precursor solution of CH_3NH_3I (Advanced Election Technology Co., Ltd) and PbI_2 (Advanced Election Technology Co., Ltd) with a molar ratio of 1 : 1 was dispersed in γ-butyrolactone and dimethyl sulfoxide (7 : 3). The perovskite active layer was prepared by spin coating on the treated substrate at 4000 rpm for 30 s. 100 μL chlorobenzene was dropped on the surface quickly in the last 7 s, after 4000 rpm was reached. The substrate was imprinted immediately using the PDMS stamp for 1–2 min and annealed at 50 and 100 °C for 3 and 25 min. Finally, an 80 nm Au layer was deposited on the perovskite layer by thermal evaporation with a shadow mask. Flat-PD, 900 nm-PD, and 180 nm-PD were fabricated under identical conditions.

Characterization

The surface morphologies of the perovskite samples were measured by field-emission SEM (HITACHI, S-4800, and Japan). XRD images were measured by an X-ray diffractometer (Rigaku, SmartLab 9kW, Japan). Absorption and reflectance spectra were recorded with a UV-vis spectrophotometer (PerkinElmer, Lambda 1050+). The optoelectronic performances under illumination at different wavelengths were recorded by a source meter (Keithley 4200A-SCS) on a four-probe station (Ideaoptics Inc). The light intensity was measured by an optical power meter (PM100D, Thorlabs). The response speed was measured by a precision source meter (Keysight B2912A).

Conclusions

In summary, we constructed a bio-inspired micro area concentrated structured perovskite photodetector by the imprinting process for good weak light detection and imaging. Its performance is attributed to light enrichment by the bio-inspired micro area concentrated structure (especially weak light harvesting), the confined crystallization resulting in high crystallinity, and a low number of defects of the perovskite. The bio-inspired micro area concentrated structured photodetector achieves high light responsivity and detectivity (0.20 A W^{-1} and 1.37×10^{13} Jones), which are 16.7 and 12.7 times higher than those of the pristine material, respectively, and the on/off ratio reaches 1×10^4. The photodetector exhibits excellent weak light detection and imaging even under the lowest light intensity (0.64 μW cm^{-2}). The results provide a new approach for the high weak light detection performance of devices.

Author contributions

L. G., K. Z. and M. T. fabricated the film and the device. L. G., R. Z. and L. G. characterized the film and device properties.

L. G. and Y. W. designed and carried out the weak light imaging. L. G., Y. W. and Y. S. wrote the article and all the authors reviewed the article.

Conflicts of interest

There are no conflicts to declare.

Acknowledgements

This research is supported by the National Natural Science Foundation of China (Grant No. 22279149, 52003273 and 51961145102), Youth Innovation Promotion Association of the Chinese Academy of Sciences (No. 2022034), National Key R&D Program of China (Grant No. 2018YFA0208501), Beijing National Laboratory for Molecular Sciences (BNLMS-CXXM-202005).

Notes and references

1 Q. Dong, Y. Fang, Y. Shao, P. Mulligan, J. Qiu, L. Cao and J. Huang, *Science*, 2015, **347**, 967–970.
2 Y. Wang, P. Wang, X. Zhou, C. Li, H. Li, X. Hu, F. Li, X. Liu, M. Li and Y. Song, *Adv. Energy Mater.*, 2018, **8**, 1702960.
3 Y. Wang, Z. Zhang, M. Tao, Y. Lan, M. Li, Y. Tian and Y. Song, *Nanoscale*, 2020, **12**, 18563–18575.
4 M. Zhang, C. Han, W.-Q. Cao, M.-S. Cao, H.-J. Yang and J. Yuan, *Nano-Micro Lett.*, 2020, **13**, 27.
5 D. Wu, H. Zhou, Z. Song, M. Zheng, R. Liu, X. Pan, H. Wan, J. Zhang, H. Wang, X. Li and H. Zeng, *ACS Nano*, 2020, **14**, 2777–2787.
6 D. Wu, Y. Xu, H. Zhou, X. Feng, J. Zhang, X. Pan, Z. Gao, R. Wang, G. Ma, L. Tao, H. Wang, J. Duan, H. Wan, J. Zhang, L. Shen, H. Wang and T. Zhai, *InfoMat*, 2022, **4**, e12320.
7 Y. Zou, T. Zou, C. Zhao, B. Wang, J. Xing, Z. Yu, J. Cheng, W. Xin, J. Yang, W. Yu, H. Dong and C. Guo, *Small*, 2020, **16**, 2000733.
8 Y. Liu, Y. Gao, J. Zhi, R. Huang, W. Li, X. Huang, G. Yan, Z. Ji and W. Mai, *Nano Res.*, 2021, **15**, 1094–1101.
9 Y. Fang and J. Huang, *Adv. Mater.*, 2015, **27**, 2804–2810.
10 A. D. Mullen, T. Treibitz, P. L. D. Roberts, E. L. A. Kelly, R. Horwitz, J. E. Smith and J. S. Jaffe, *Nat. Commun.*, 2016, **7**, 12093.
11 J. S. Jaffe, P. J. Franks, P. L. Roberts, D. Mirza, C. Schurgers, R. Kastner and A. Boch, *Nat. Commun.*, 2017, **8**, 14189.
12 Z. Ji, G. Cen, C. Su, Y. Liu, Z. Zhao, C. Zhao and W. Mai, *Adv. Opt. Mater.*, 2020, **8**, 2001436.
13 Y. Wang, Y. Lan, Q. Song, F. Vogelbacher, T. Xu, Y. Zhan, M. Li, W. E. I. Sha and Y. Song, *Adv. Mater.*, 2021, **33**, 2008091.
14 Y. Wu, E. A. Hadly, W. Teng, Y. Hao, W. Liang, Y. Liu and H. Wang, *Sci. Rep.*, 2016, **6**, 33578.
15 Q. Song, Y. Wang, F. Vogelbacher, Y. Zhan, D. Zhu, Y. Lan, W. Fang, Z. Zhang, L. Jiang, Y. Song and M. Li, *Adv. Energy Mater.*, 2021, **11**, 2100742.
16 C. Li, M. Zhao, X. Zhou, H. Li, Y. Wang, X. Hu, M. Li, L. Shi and Y. Song, *Adv. Opt. Mater.*, 2018, **6**, 1800651.
17 Z. Huang, M. Su, Q. Yang, Z. Li, S. Chen, Y. Li, X. Zhou, F. Li and Y. Song, *Nat. Commun.*, 2017, **8**, 14110.
18 F. Cao, W. Tian, M. Wang, H. Cao and L. Li, *Adv. Funct. Mater.*, 2019, **29**, 1901280.
19 M. Wang, Y. Zuo, J. Wang, Y. Wang, X. Shen, B. Qiu, L. Cai, F. Zhou, S. P. Lau and Y. Chai, *Adv. Energy Mater.*, 2019, **9**, 1901801.
20 M. Du, X. Zhu, L. Wang, H. Wang, J. Feng, X. Jiang, Y. Cao, Y. Sun, L. Duan and Y. Jiao,, *Adv. Mater.*, 2020, **32**, 2004979.
21 W. Kim, M. S. Jung, S. Lee, Y. J. Choi, J. K. Kim, S. U. Chai, W. Kim, D. G. Choi, H. Ahn and J. H. Cho, *Adv. Energy Mater.*, 2018, **8**, 1702369.
22 W. Wang, Y. Ma and L. Qi, *Adv. Funct. Mater.*, 2017, **27**, 1603653.
23 H. Wang, R. Haroldson, B. Balachandran, A. Zakhidov, S. Sohal, J. Y. Chan, A. Zakhidov and W. Hu, *ACS Nano*, 2016, **10**, 10921–10928.
24 W. Kong, S. Wang, F. Li, C. Zhao, J. Xing, Y. Zou, Z. Yu, C. H. Lin, Y. Shan, Y. H. Lai, Q. Dong, T. Wu, W. Yu and C. Guo, *Adv. Energy Mater.*, 2020, **10**, 2000453.
25 J. Song, L. Xu, J. Li, J. Xue, Y. Dong, X. Li and H. Zeng, *Adv. Mater.*, 2016, **28**, 4861–4869.
26 X. Fu, Q. Wang, J. Wang, Z. Huang, X. Li, D. Wen, J. Fang, B. Li, S. Zhou and H. Zhang, *J. Mater. Chem. C*, 2021, **9**, 13704–13712.
27 P. Zhang, L. Liang and X. Liu, *J. Mater. Chem. C*, 2021, **9**, 16110–16131.
28 Y. Wang, M. Li, X. Zhou, P. Li, X. Hu and Y. Song, *Nano Energy*, 2018, **51**, 556–562.
29 H. Sun, W. Tian, F. Cao, J. Xiong and L. Li, *Adv. Mater.*, 2018, **30**, 1706986.
30 S. F. Leung, K. T. Ho, P. K. Kung, V. K. S. Hsiao, H. N. Alshareef, Z. L. Wang and J. H. He, *Adv. Mater.*, 2018, **30**, 1704611.
31 X. Gong, M. H. Tong, Y. J. Xia, W. Z. Cai, J. S. Moon, Y. Cao, G. Yu, C.-L. Shieh, B. Nilsson and A. J. Heeger, *Science*, 2009, **325**, 1665–1667.
32 Q. Zhang, M. Shou, Y. Xu, J. Zheng, X. Wen, Y. Zhao, H. Wang, L. Liu and Z. Xie, *J. Mater. Chem. C*, 2020, **8**, 16506–16512.
33 Y. Pan, H. Wang, X. Li, X. Zhang, F. Liu, M. Peng, Z. Shi, C. Li, H. Zhang, Z. Weng, M. Gusain, H. Long, D. Li, J. Wang, Y. Zhan and L. Zheng, *J. Mater. Chem. C*, 2020, **8**, 3359–3366.
34 C. Shan, F. Meng, J. Yu, Z. Wang, W. Li, D. Fan, R. Chen, H. Ma, G. Li and A. K. K. Kyaw, *J. Mater. Chem. C*, 2021, **9**, 7632–7642.
35 W. Zheng, R. Lin, Z. Zhang, Q. Liao, J. Liu and F. Huang, *Nanoscale*, 2017, **9**, 12718–12726.
36 G. Xiong, Z. Qin, B. Li, L. Wang, X. Zhang, Z. Zheng, H. Zhu, S. Zhao, J. Gao, B. Li, J. Yang, X. Li, J. Luo, Z. Han, X. Liu and F. Zhao, *J. Mater. Chem. C*, 2021, **9**, 2095–2105.
37 X. Liu, Z. Liu, J. Li, X. Tan, B. Sun, H. Fang, S. Xi, T. Shi, Z. Tang and G. Liao, *J. Mater. Chem. C*, 2020, **8**, 3337–3350.

38 Y. Liu, F. Li, C. Perumal Veeramalai, W. Chen, T. Guo, C. Wu and T. W. Kim, *ACS Appl. Mater. Interfaces*, 2017, **9**, 11662–11668.
39 F. Quinlan, T. M. Fortier, H. Jiang, A. Hati, C. Nelson, Y. Fu, J. C. Campbell and S. A. Diddams, *Nat. Photonics*, 2013, **7**, 290–293.
40 Y. Fang, A. Armin, P. Meredith and J. Huang, *Nat. Photonics*, 2018, **13**, 1–4.
41 H. Deng, X. Yang, D. Dong, B. Li, D. Yang, S. Yuan, K. Qiao, Y. B. Cheng, J. Tang and H. Song, *Nano Lett.*, 2015, **15**, 7963–7969.
42 H. Deng, D. Dong, K. Qiao, L. Bu, B. Li, D. Yang, H. E. Wang, Y. Cheng, Z. Zhao, J. Tang and H. Song, *Nanoscale*, 2015, **7**, 4163–4170.
43 S. Lim, M. Ha, Y. Lee and H. Ko, *Adv. Opt. Mater.*, 2018, **6**, 1800615.